Research Square

Preprints are preliminary reports that have not undergone peer review.
They should not be considered conclusive, used to inform clinical practice,
or referenced by the media as validated information.

Time-dependent toxicity of potassium peroxymonosulfate to the microalga Chlorella pyrenoidosa: implications for aquaculture disinfection practice

Yi Du
Yangzhou University
Le kong
Yangzhou University
Qiyan Cao
Yangzhou University
Haiyong Zhao
Jiangsu Yongrong Biotechnology Co., Ltd
Wenzhi Wei
wzwei@yzu.edu.cn
Yangzhou University

Research Article

Keywords: Potassium peroxymonosulfate, Chlorella pyrenoidosa, dynamics of decomposition product, Cellular damage, Oxidative stress, Transcriptomics

Posted Date: November 25th, 2026

DOI: https://doi.org/10.21203/rs.3.rs-11685303/v1

License: This work is licensed under a Creative Commons Attribution 4.0 International License.
Read Full License

Additional Declarations: No competing interests reported.

Time-dependent toxicity of potassium peroxymonosulfate to the microalga Chlorella pyrenoidosa: implications for aquaculture disinfection practice

Yi Du[a], Le kong[a], Qiyan Cao[a], Haiyong Zhao[b], Wenzhi Wei[a]*

[a]College of Animal Science and Technology, Yangzhou University, Yangzhou 225009, Jiangsu, China

[b]Jiangsu Yongrong Biotechnology Co., Ltd., Huai'an 223001, Jiangsu, China

*Corresponding author: wzwei@yzu.edu.cn

Abstract: The widespread use of potassium peroxymonosulfate (PMS) in aquaculture raises concerns about its environmental risks.This study evaluated the toxic effects of PMS on the microalga *Chlorella pyrenoidosa*, a species with multiple functional applications in aquaculture water bodies. By testing the effects of PMS on its growth and other parameters, the impact of PMS disinfection in aquaculture practice on the primary productivity of aquaculture water bodies can be assessed. All experimental groups (PMS concentrations of 0, 1.70, 3.40, 8.49 mg L^{-1}, corresponding to 0, 0.1, 0.2 and 0.5 times of the 96 h EC_{50}, respectively) were cultured for 12 days, and indicators were performed on day 0, 3, 6, 9, and 12. The cell growth, oxidative stress, ultrastructure, chlorophyll fluorescence, transcriptomic gene express, and PMS decomposition products were measured. The results indicated that PMS inhibited the growth of *C.pyrenoidosa* cells, decreased photosynthetic pigment contents, reduced chlorophyll fluorescence parameters, and induced cellular structural damage (e.g., surface shrinkage, plasmolysis, chloroplast damage, thylakoid disorganization), accompanied by elevated oxidative stress and down-regulation of genes related to growth and protein synthesis.Notably, all inhibitory effects peaked on day 3 and subsequently recovered gradually, exhibiting a significant time-dependent toxic effect. These phenomena were significantly correlated with the decomposition products of

PMS (H_2O_2, •OH, SO_4^{2-}, and ClO^-), indicating that the dynamic changes in the concentrations of PMS decomposition products drive the time-dependent toxic effects of PMS on *C.pyrenoidosa*. These findings provide insights for the safe application of PMS in aquaculture disinfection practice.

Keywords: Potassium peroxymonosulfate; *Chlorella pyrenoidosa*; dynamics of decomposition product; Cellular damage; Oxidative stress; Transcriptomics

Highlights:

1. Exposure to PMS inhibits the growth performance of *C.pyrenoidosa*, due to oxidative stress and cell damage induced by its rapid decomposition products.

2. Concentration changes of PMS decomposition products cause time-dependent toxicity: growth inhibition of *C.pyrenoidosa* on day 3 followed by recovery.

3. Transcriptomic analysis of differentially expressed genes (DEGs) validated the changes in growth indicators of *C.pyrenoidosa*.

1.Introduction

China is the world's largest aquaculture producer. By 2024, its total aquaculture output has ranked first globally for more than 30 consecutive years (FDMA, 2025; Xu et al., 2023). Among various aquaculture methods, pond aquaculture is the predominant one, contributing approximately 70% of the country's total freshwater aquaculture production (Zhao and Shen, 2016). However, as pond farming increasingly shifts toward intensive, high-density models, the organic load from residual feed and feces continues to rise, leading to deterioration of water quality in aquaculture systems and frequent disease outbreaks. This has forced practitioners to extensively use various disinfectants to control the spread of pathogenic microorganisms. Although disinfectants can effectively suppress diseases in the short term, long-term or excessive use may lead to toxic effects on cultured organisms and non-target microorganisms, disrupting the microecological balance of the water, and potentially inducing antimicrobial resistance (Ng and Mont, 2025). These issues pose

non-negligible secondary hazards to the aquaculture environment and surrounding ecosystems. Therefore, while ensuring aquaculture productivity, it is urgently necessary to assess the ecological risks of disinfectants and to explore more green and sustainable strategies for disease prevention and control.

Potassium peroxymonosulfate (PMS), with the chemical formula $2KHSO_5 \cdot KHSO_4 \cdot K_2SO_4$, is a versatile oxidizing agent that has attracted considerable attention as an advanced disinfectant. PMS can be readily activated through various methods, such as UV photolysis, electrolysis, thermal treatment, ultrasound, and transition metal oxide catalysis—thereby decomposing to produce hydroxyl radicals (•OH), sulfate radicals ($SO_4^{\bullet -}$), and hydrogen peroxide (H_2O_2) (Yu et al., 2020; Zheng et al., 2022). These reactive species target microbial cell membranes, elevate intracellular ROS levels, disrupt cellular structures, and ultimately lead to cell inactivation (Tian et al., 2024). Compared to traditional disinfectant like hydrogen peroxide and ozone, PMS offers advantages in terms of higher stability, cost-effectiveness, non-toxicity, safety, and ease of storage and transportation (Liu et al., 2017; Luo et al., 2021; Mohammadi et al., 2021). Consequently, PMS has been employed as a disinfectant in diverse sectors, including aquaculture, swimming pool water treatment, and food hygiene and safety (Anipsitakis et al., 2008; Wang et al., 2020).

In the aquaculture industry, the primary applications of PMS are pathogen inactivation, organic pollutant degradation, and in-situ sediment remediation. For example, PMS at 0.5% completely inactivates LSHV-2 virus within one minute, outperforming povidone-iodine and hydrogen peroxide (Johnston et al., 2024). UV/C (10 W/m^2) combined with PMS (0.1 mM) achieved nearly 100% inactivation of *Enterococcus faecalis* within one minute and degraded over 80% of amoxicillin in real aquaculture water within 45 minutes, demonstrating its dual potential for disinfection and antibiotic degradation (Santiago-Espiñeira et al., 2025). Moreover, PMS treatment has been reported to significantly reduce sedimentary nitrogen loads—particularly ammonium (NH_4^+)—indicating its capacity to mitigate

endogenous nitrogen pollution and alleviate nitrogen-induced toxicity in aquaculture water (Yin et al., 2026).

Chlorella pyrenoidosa, a freshwater unicellular green algal, occupies a foundational position in aquatic food webs as a primary producer. Due to its high sensitivity to aquatic pollutants, ease of cultivation, rapid growth cycle, and well-characterized physiological responses, *C.pyrenoidosa* has become a widely adopted model organism in ecotoxicity testing (Liu et al., 2019; Zhang et al., 2025; Zhao et al., 2017). This beneficial microalgal also plays multiple functional roles in aquaculture: it serves as a nutrient-rich live feed for larval stages (Deng et al., 2021; Zeng et al., 2023), removes organic and inorganic pollutants from culture water (Hao et al., 2025), and contributes to the competitive inhibitor of harmful algal blooms (Peng et al., 2025). Although *C.pyrenoidosa*, as a multifunctional microalga, is essential to the aquaculture water environment and productivity, the time-dependent toxicity of commonly used disinfectants to this alga remains poorly understood, particularly when intensive use of aquaculture disinfectants is unavoidable in production.

Our study aims to reflect the impact of PMS on the primary productivity of aquaculture water bodies in practice by investigating its effects on *C.pyrenoidosa*. Firstly, the 96-hour median inhibition concentration (EC_{50}) of PMS on *C.pyrenoidosa* cells were determined in preliminary experiments. Secondly, the concentration gradient of PMS for the long-term toxicity test were decided according to safe concentration.By measuring the growth performance, chlorophyll content, cellular structure, oxidative stress, and transcriptomic gene expression of *C.pyrenoidosa*, as well as PMS decomposition products, this study elucidated the changing trend and underlying mechanisms of PMS toxicity to this microalga, and simultaneously explored the relationship between the dynamics of PMS decomposition product concentrations and the variation in this toxic effect. The findings of this study will provide an important basis for an in-depth understanding of the toxicity of PMS to *C.pyrenoidosa* and offer guidance for the application of PMS in aquaculture disinfection practice.

2.Materials and methods

2.1 Materials

Potassium peroxymonosulfate (PMS, with a purity of ≥99 %) was purchased from Shanghai Yien Chemical Technology Co., Ltd, China. The protein quantification assay kit, malondialdehyde (MDA) assay kit, catalase (CAT) assay kit, superoxide dismutase (SOD) assay kit, and glutathione peroxidase (GSH-PX) assay kit used for oxidative stress determination were all purchased from Nanjing Jiancheng Bioengineering Institute, China. Their catalog numbers are No. A045-2-2, No. A003-1-2, No. A007-1-2, No. A001-3-2, and No. A005-1-2, respectively. In addition, the reactive oxygen species (ROS) assay was performed using an enzyme-linked immunosorbent assay (ELISA) kit purchased from Jiangsu Meimian Industrial Co., Ltd., China.

C.pyrenoidosa (FACHB-9) were obtained from the Freshwater Algal Culture Collection at the Institute of Hydrobiology (FACHB Collection Center; Wuhan, China). *C.pyrenoidosa* were cultivated in BG11 medium at a temperature of 22 ± 1 ℃, with a light intensity of 5000 Lux and a light-dark cycle of 13 :11. To ensure uniform cell suspension and minimize sedimentation-induced light limitation, culture flasks were gently agitated twice daily (morning and evening).

2.2 Acute toxicity test

For acute exposure experiments, 200 mL aliquots of exponentially growing *C.pyrenoidosa* cultures were transferred into sterile 250 mL glass beakers. Potassium peroxymonosulfate (PMS) was added to achieve different concentration gradients (1, 2, 4, 8, 16, and 32 mg L^{-1}). Each treatment included four biological replicates. Cultures were incubated for 96 h, and algal cell density was quantified every 24 h by spectrophotometric measurement of optical density at 680 nm (OD_{680}). The regression curve between the number of *C.pyrenoidosa* cells and absorbance value was calculated, and cell densities were derived from a linear calibration curve relating OD_{680} to cell count (R^2=0.98).

$$Y=5994871X-361909 \quad (1)$$

Where Y: Number of *C.pyrenoidosa* cells (10^6/ml); X: Absorbance value

The median effective concentration (EC_{50}) values at 24 h, 48 h, 72 h, and 96 h, along with their 95% confidence intervals (CI), were calculated by probit analysis in SPSS 18.

2.3 Chronic Toxicity Test

Based on the 96 h EC_{50} value of 16.98 mg L^{-1}, three sublethal concentrations were selected for the chronic toxicity test: 1.70 mg L^{-1} (0.1 × EC_{50}), 3.40 mg L^{-1} (0.2 × EC_{50}), and 8.49 mg L^{-1} (0.5 × EC_{50}). Subsequently, the cells were continuously cultured for 12 days, and the absorbance at 680 nm was measured at 0, 3, 6, 9, and 12 days of culture. Each experimental group was tested for four repetitions.

2.3.1 The inhibition rate

The toxic effect of PMS on *C.pyrenoidosa* was expressed as the inhibition rate, which was calculated using Eq. 2.

$$Ir = (C0-Ct)/C0 \quad (2)$$

Where C0: Cell density at time 0; Ct: Cell density at time t.

2.3.2 Pigment measurement

Pigment content served as an indicator of the biomass of *C.pyrenoidosa* (Vishwakarma et al., 2023). The trends in the contents of chlorophyll a (Chl a), chlorophyll b (Chl b), and carotenoids (Car) were used to further reflect the toxic effects of PMS on *C.pyrenoidosa*. The determination and calculation of Chl a, Chl b, and Car were performed following the methods described in previous work (Damergi et al., 2017).

2.3.3 Observation of cell structure and morphology

For each treatment, 20 mL of mid-log-phase culture was harvested by centrifugation (4500× g, 10 min, 4 °C). Samples were initially fixed 24 h at 4 °C with 2.50% glutaraldehyde and then washed three times with phosphate-buffered saline (PBS, pH=7.4). Afterward, the samples were dehydrated for 15 min through a series of 30, 50, 70, 80, 90, 95, and 100% alcohol solutions. The dehydrated samples were placed in an oven at 40°C and dried for 24 h. After gold spraying, the surface morphology of *C.pyrenoidosa* cells were observed by scanning electron microscopy (SEM; Zeiss sigma 300, Germany) (Z. Li et al., 2022).

Internal ultrastructure was analyzed by transmission electron microscopy (TEM; Hitachi HT7800, Japan). Similarly, 20 mL cultures were centrifuged (1000× g, 15 min, 4 °C), and pellets were fixed sequentially in 2.5% glutaraldehyde and 1% osmium tetroxide (in 0.1 M phosphate buffer, pH 7.4) for 4 h at 4 °C. Samples were then dehydrated in ethanol-acetone mixtures, infiltrated with EPON 812 resin, embedded, sectioned (70-90 nm), and stained with uranyl acetate and lead citrate before TEM observation (Zhou et al., 2012).

2.3.4 Determination of chlorophyll fluorescence intensity, and cell and particle size

C.pyrenoidosa samples were collected from each treatment group at 0, 3, 6, 9, and 12 days for flow cytometric analysis. The specific operation was as follows: 1mL of the culture in each group was centrifuged at 4 ℃ 3000× g for 10 min, and the supernatant was removed, the algal cells were collected. After repeating 3 times, the algal cells were resuspended with PBS and analyzed via on a flow cytometer (FACS LSRFortessa, BD, USA) at a flow rate of 66 μL min^{-1}. This chlorophyll content was detected through flow cytometry FL3 channel (excitation wavelength: 488 nm, emission wavelength: 677 nm). The chlorophyll fluorescence intensity value was expressed by the fluorescence intensity value of percp-cy 5.5 whose emission wavelength was close to 680 nm. The values of forward-angle light scatter (FSC) and side-angle light scatter (SSC) were measured to reflect the cell and particle sizes, and morphological changes in algal cells, respectively (Cao et al., 2023).

2.3.5 Measurement of oxidative stress

From each group, 50 mL of algal culture was collected and centrifuged at 5000 × g for 10 min at 4 °C. The supernatant (culture medium) was discarded, and an appropriate amount of the cell pellet (containing > 10^6 cells/mL after resuspension) was retained. The cells were resuspended in 0.3 mL of 0.1 mol/L phosphate-buffered saline (PBS) and subjected to ultrasonic disruption in an ice-water bath (power: 300 W; ultrasonication cycle: 5 s on, 15 s off; repeated six times). The resulting homogenate was centrifuged again at 5000 × g for 10 min at 4 °C, and the supernatant was collected for subsequent analyses (Xiang and Zhou, 2023). All subsequent operations were performed in accordance with the requirements of the manufacturers of the corresponding kits for each indicator.

2.3.6 Determination of PMS decomposition components

PMS decomposition byproducts include •OH, sulfate ions (SO_4^{2-}), H_2O_2, and hypochlorite ions (ClO^-), among other components. In this experiment, the •OH was determined using the Fenton reaction colorimetric method (Adachi et al., 2022). The SO_4^{2-} concentration was determined using the barium chloride precipitation method (Vijayakumar and Dawson, 2024). The H_2O_2 levels was determined using the N,N'-diethyl-p-phenylenediamine (DPD) colorimetric method (Zou et al., 2019). And the ClO^- concentration was determined using the DPD colorimetric method (Salami et al., 2008).

2.3.7 high-throughput transcriptome sequencing

The specific experimental procedures were as follows: From each group, a 50 mL sample was collected and centrifuged at 1500× g for 10 min at 4 °C. The culture medium was discarded, and the algal cell pellet was retained. Then, 1ml PBS buffer was added and centrifuged at 4 ℃ 1500× g for 10 min. The supernatant was removed, and the resulting cell pellets were handed over to Shanghai Oebiotech Co., Ltd. for further analysis. The pretreatment of the samples before submission was carried out in accordance with the requirements of the company.

The differentially expressed gene (DEGs) analysis data obtained by comparing each concentration experimental group with the control group at day 3 of cultivation have been deposited in the NCBI GEO database under accession number GSE330137 (https://www.ncbi.nlm.nih.gov/geo/query/acc.cgi?acc=GSE330137). The DEGs analysis data obtained by comparing the 0.5 × EC_{50} experimental group at 0, 3, 6, 9, and 12 days with the control group at day 0 of cultivation have been deposited in the NCBI GEO database under accession number GSE329134 (https://www.ncbi.nlm.nih.gov/geo/query/acc.cgi?acc=GSE329134).

2.4 Data analysis

The results were expressed as mean ± standard deviation (mean ± SD). One-way analysis of variance (ANOVA) was subsequently performed to assess differences among group means. Tukey's multiple comparison test was used to determine statistically significant differences between groups, with a significance level set at $p<0.05$. All statistical analyses and graphical representations were conducted using SPSS (version 18), Microsoft Excel, and Origin (version 2025).

3. Results

3.1 Acute toxicity of PMS on *C.pyrenoidosa*

The inhibition rate of *C.pyrenoidosa* in the acute toxicity test exhibited a clear dose-response relationship (Table 1). The 24, 48, 72, and 96 h median effective concentration (EC_{50}) values of PMS were 31.41 (20.32-48.53), 23.55 (16.24-34.28), 21.33 (16.24-28.01), and 16.98 (11.57-24.92) mg L^{-1}, respectively. With the time increased, the 50% inhibition rate of *C.pyrenoidosa* happened at a lower concentration of PMS.

206 Table.1 Median inhibitory concentration (EC_{50}) in mg L^{-1} of PMS for the 24 h-96 h acute
207 toxicity

Time (hrs)	Probit equation	EC_{50}[a]	R^2
24	P =1.359 x+0.817	31.41(20.32-48.53)	0.978
48	P = 1.312 x+0.716	23.55(16.18-34.28)	0.980
72	P = 0.519 x+1.070	21.33(16.24-28.01)	0.988
96	P = 0.383 x+1.039	16.98(11.57-24.92)	0.971

208
209 a: Values in parentheses represent 95% confidence intervals (CIs)

210 **3.2 Chronic toxicity test of PMS on *C.pyrenoidosa***

211 After 12 days of potassium peroxymonosulfate (PMS) treatment, the most
212 significant differences in cell density of *C.pyrenoidosa* between the control and
213 experimental groups were observed on day 3 (P<0.05) (Fig. 1a). Compared to the
214 control, the growth of the microalgal in the experimental groups was significantly
215 inhibited during the first 3 days, with the inhibitory effect strengthening as the PMS
216 concentration increased. Specifically, compared with the control group, the cell
217 densities in the experimental groups decreased by 30.6%, 46.0%, and 81.3% on day 3,
218 corresponding to low, medium, and high PMS concentrations, respectively. This
219 inhibitory effect gradually weakened and eventually disappeared between days 6 and
220 12.

221 The determination results of all pigment content of *C.pyrenoidosa* after 12 days
222 of culture were shown in Fig. 1b-d. The experimental group was significantly
223 inhibited from 0 to 3 days compared with the control group, and the inhibitory effect
224 disappeared from 6 to 12 days, and the inhibitory effect was a generally
225 dose-dependent relationship with the concentration of PMS (P<0.05).

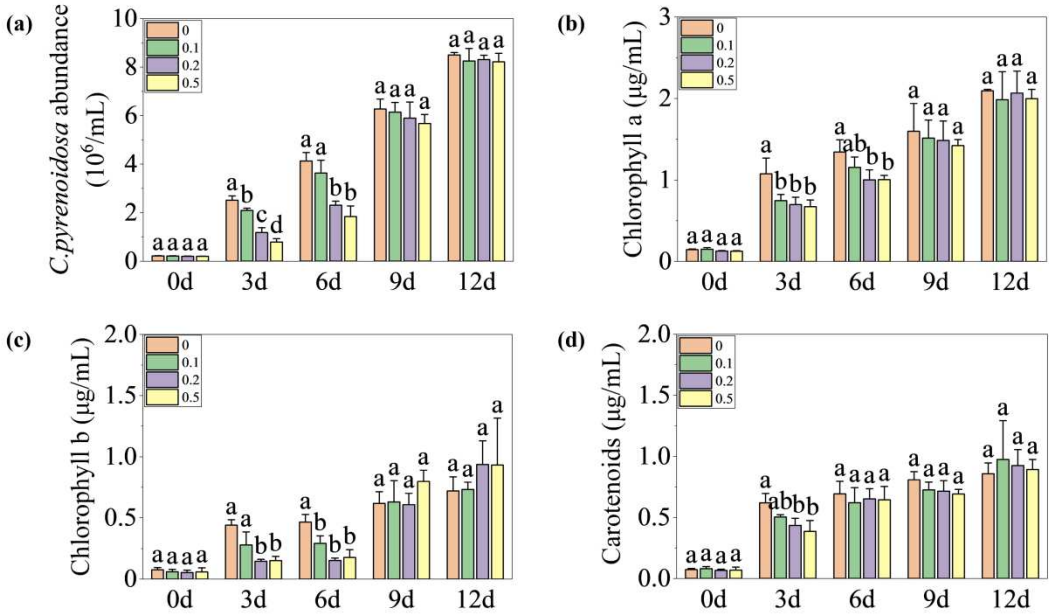


Fig. 1 Effect of different concentrations of PMS on the growth and pigment content of *C.pyrenoidosa*. The above indicators were determined by spectrophotometry. (a) 0-12 d *C.pyrenoidosa* cell abundance; (b) 0-12 d *C.pyrenoidosa* cell chlorophyll a content; (c) 0-12 d *C.pyrenoidosa* cell chlorophyll b content; (d) 0-12 d *C.pyrenoidosa* cell carotenoids content. A significance level of $P < 0.05$ was used for all comparisons.

3.3 Determination of chlorophyll fluorescence intensity, and cell and particle size

Forward scatter signal (FSC) intensity directly reflects relative cell size, while side scatter (SSC) correlates with intracellular granularity or particle content (Ganguly et al., 2020). The variation trends in algal cell volume in both the experimental and control groups were characterized by an initial increase followed by a decrease (Fig. 2a). Notably, during the period from day 0 to day 3, the FSC values in the experimental groups were generally higher than those in the control group, with the 0.5 × EC_{50} concentration group showing a significant increase compared to the control (P<0.05). In contrast, from day 6 to day 12, the FSC values in the experimental groups gradually fell below those of the control group. In addition, Intracellular particle content in both the experimental and control groups increased initially and then decreased, with no significant differences observed overall between the groups (Fig. 2b).

The variation trend of chlorophyll fluorescence intensity can reflect the efficiency of light energy utilization by photosystem II (PSII) and the degree of

photodamage to PSII (Maxwell and Johnson, 2000). On day 3 of cultivation, the 0.5 × EC_{50} group exhibited significantly higher chlorophyll fluorescence intensity than the control group, while no significant differences were observed in the other experimental groups (P<0.05) (Fig. 2c). Subsequently, from day 6 to day 12, chlorophyll fluorescence intensity in the experimental groups gradually declined.

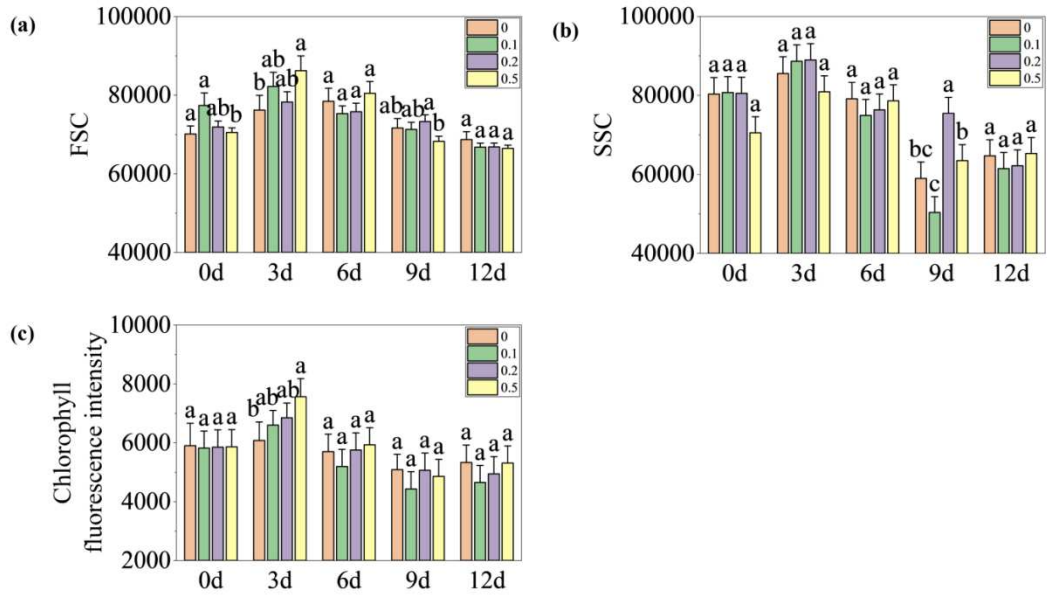


Fig. 2 Effect of different concentrations of PMS on the chlorophyll fluorescence intensity and Forward scatter signal (FSC)/side scatter (SSC) values of *C.pyrenoidosa*. The chlorophyll fluorescence intensity and related parameters of *C.pyrenoidosa* in each group from day 0 to day 12 were determined using flow cytometry. (a) 0-12 d all group FSC value; (b) 0-12 d all group SSC value; (c) 0-12 d all group chlorophyll fluorescence. A significance level of $P < 0.05$ was used for all comparisons.

3.4 Electron microscopic observation of cell morphology and structure

SEM images of *C.pyrenoidosa* cells under different concentrations of PMS stress were shown in Fig. 3 a-g. In the control group (Fig. 3a), the algal cell surfaces appeared intact without obvious wrinkling. After 3 days of exposure to varying PMS concentrations, the cell surfaces exhibited different degrees of damage (Fig. 3b-d). Cells in the 0.1 × EC_{50} group showed slight surface wrinkling but remained largely intact (Fig. 3b). In the 0.2 × EC_{50} group, the surface of *C.pyrenoidosa* cells displayed pronounced wrinkling, minor surface breakage, and slight deformation (Fig. 3c). Cells in the 0.5 × EC_{50} group developed a granular appearance on the surface, along with

severe wrinkling and obvious deformation (Fig. 3d). These observations indicated that PMS stress leads to significant alterations in the surface structure of *C.pyrenoidosa* cells. The surface morphology of algal cells in the 0.5 × EC_{50} group after 6, 9, and 12 days of PMS exposure was presented in Fig. 3e-g. Compared with the control group, the surface damage in the 0.5 × EC_{50} group gradually diminished, and cell shape progressively approached that of the control.

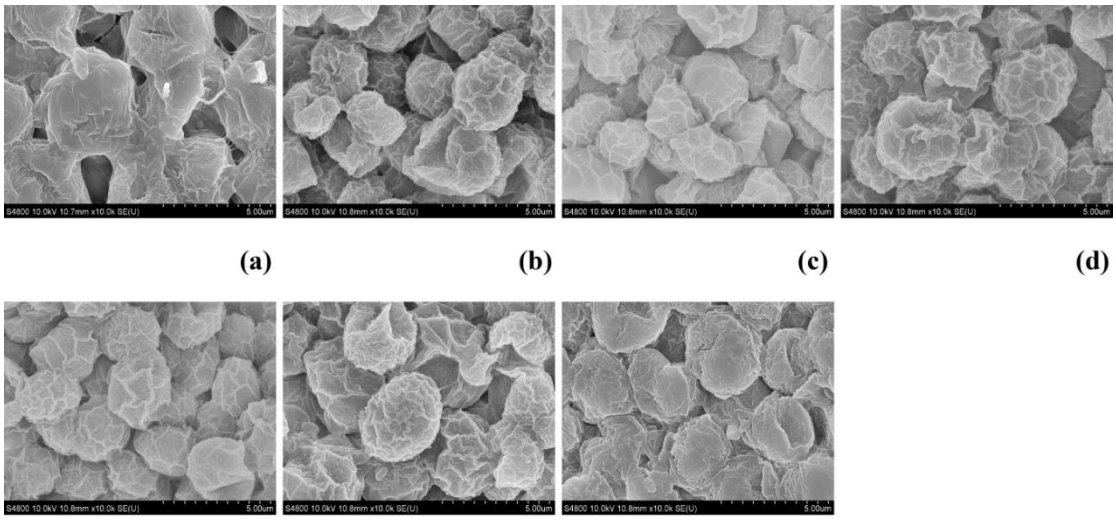


Fig. 3a-g Scanning electron microscope (SEM) image of *C.pyrenoidosa.* The surface morphological structures of *C.pyrenoidosa* cells in each group on day 3 and those in the 0.5 × EC_{50} group from day 6 to day 12 were photographed using SEM. (a-d) SEM images of *C.pyrenoidosa* in each group on day 3; (e-g) The SEM images of *C.pyrenoidosa* cells in the 0.5 × EC_{50} group on days 6, 9, and 12 are shown in Figures e, f, and g, respectively.

TEM images of *C.pyrenoidosa* cells under varying concentrations of PMS stress were presented in Fig. 3h-n. Observation of the control group (Fig. 3h) revealed broadly oval algal cells with thick and intact cell walls. Nucleoli and nuclear membranes were clearly visible within the nucleus, and the cells contained well-defined cup-shaped chloroplasts and vacuoles. Distinct alterations in the internal structure of *C.pyrenoidosa* cells were observed after 3 days of exposure to different PMS concentrations (Fig. 3i-k). Figure 3i showed that the 0.1 × EC_{50} group exhibited thickened cell walls while the cellular structure remained largely intact. Figure 3j illustrated deformed cells in the 0.2 × EC_{50} group, with gaps in the cell wall leading to

content leakage, slight plasmolysis, disrupted chloroplast integrity, and disorganized thylakoid membrane systems. Fig. 3k demonstrated that cells in the 0.5 × EC_{50} group were deformed, with ruptured cell walls and content leakage, accompanied by mild plasmolysis, swollen chloroplasts, disordered thylakoid membranes, damaged starch sheaths, and the appearance of numerous lipid droplets. Thus, PMS stress caused damage to the internal structures of *C.pyrenoidosa* cells. The internal structures of algal cells in the 0.5 × EC_{50} group after 6, 9, and 12 days of PMS exposure were shown in Figures 3 l-n. Compared with the control group, a gradual recovery of cellular damage was evident in the 0.5 × EC_{50} group, manifested as the restoration of cell shape, reconstruction of the pyrenoid structure, and disappearance of plasmolysis.

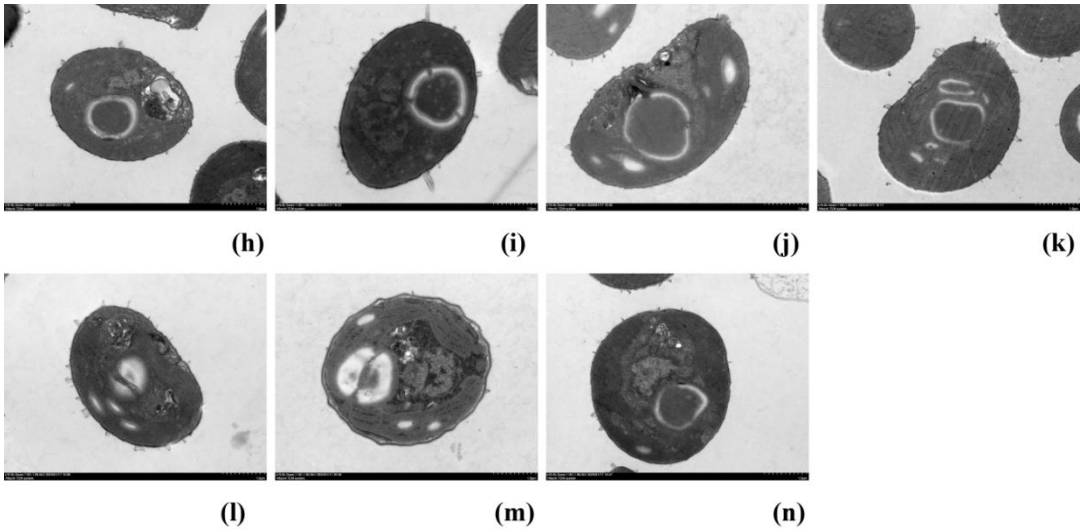


Fig. 3h-n Transmission electron microscopy (TEM) image of *C.pyrenoidosa.* The internal morphological structures of *C.pyrenoidosa* cells in each group on day 3 and those in the 0.5 × EC_{50} group from day 6 to day 12 were photographed using TEM. (h-k) TEM images of *C.pyrenoidosa* in each group on day 3; (l-n) The TEM images of *C.pyrenoidosa* cells in the 0.5 × EC_{50} group on days 6, 9, and 12 are shown in Figures e, f, and g, respectively.

3.5 Oxidative stress responses

After three consecutive days of cultivation, the reactive oxygen species (ROS) content in the 0.1 × EC_{50}, 0.2 × EC_{50} and 0.5 × EC_{50} groups significantly increased by 2.5%, 10.4%, and 24.3% compared to the control group (P<0.05) , respectively (Fig. 4a). Thereafter, from day 6 to day 12, the ROS content in each experimental group gradually declined to levels showing no significant difference from the control group. Meanwhile, MDA exhibited a similar trend of change as ROS, whereas PMS exerted

a greater impact on MDA. After three consecutive days of culture, the malondialdehyde (MDA) content in the experimental groups increased by 41.7%, 97.3%, and 230.8% from low to high concentrations, respectively (Fig. 4b).

In all concentration-based experimental groups, the activities of antioxidant enzymes, including catalase (CAT), superoxide dismutase (SOD) and glutathione peroxidase (GSH-PX) in *C.pyrenoidosa* were generally significantly lower than those in the control group during days 3 (P<0.05) (Fig. 4c-e). Subsequently, from day 6 to day 12, they gradually recovered until no significant difference was observed compared to the control group.

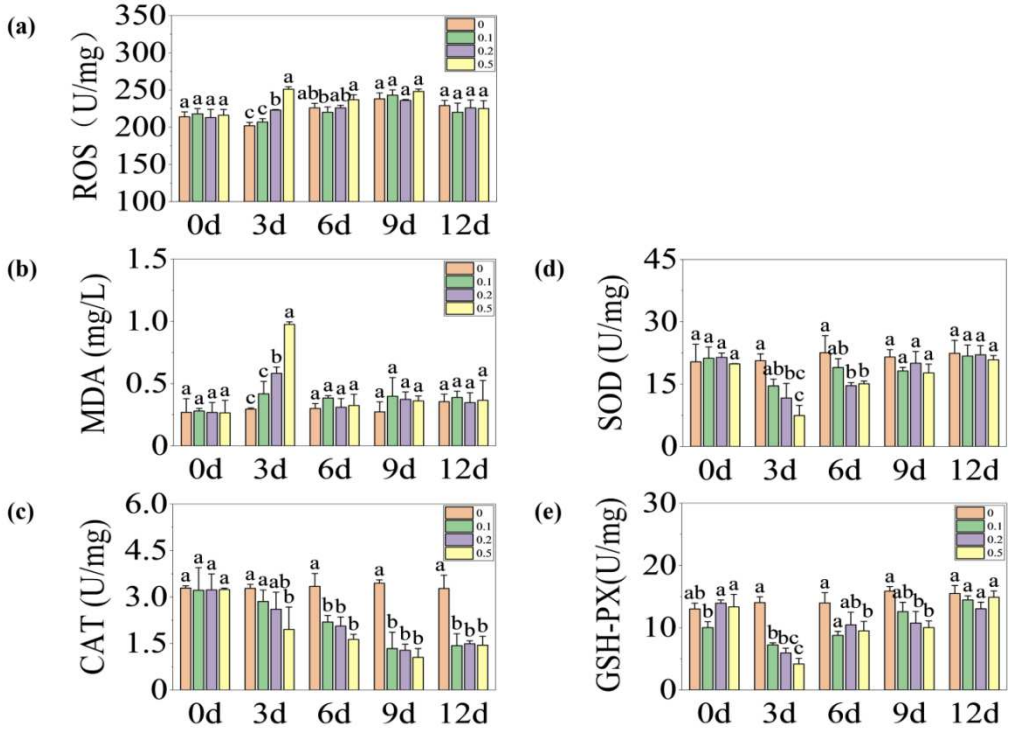


Fig. 4 Effect of different concentrations of PMS on the degree of oxidative stress in *C.pyrenoidosa.* All indicators shown in this figure were determined according to the instructions provided by the manufacturers of the corresponding kits. (a) 0-12 d all group ROS content; (b) 0-12 d all group MDA content; (c) 0-12 d all group CAT activity; (d) 0-12 d all group SOD activity; (e) 0-12 d all group GSH-PX activity. A significance level of $P < 0.05$ was used for all comparisons.

3.6 PMS decomposition component content

In all experimental groups, the concentrations of hydrogen proxide (H_2O_2) and hydroxyl radical (•OH) exhibited a trend of initially increasing significantly compared to the control group (3-6 d) (P<0.05), followed by a decrease to levels showing no significant difference from those of the control group (9-12 d) (Fig. 5a-b).

The change trend of sulfate ions (SO_4^{2-})concentration showed a different pattern from that of H_2O_2 and •OH. The SO_4^{2-} concentration in the high PMS group was always significantly higher than that in the blank group (P<0.05), and by the day 12, with the increase of PMS concentration, the SO_4^{2-} concentration showed a significantly increasing trend (P<0.05) (Fig. 5c). The ClO^- level in the experimental groups was significantly higher than that in the control on the 0 day of cultivation (P<0.05) (Fig. 5d). During days 3-12, the ClO^- content in both the experimental and control groups decreased rapidly and approached zero.

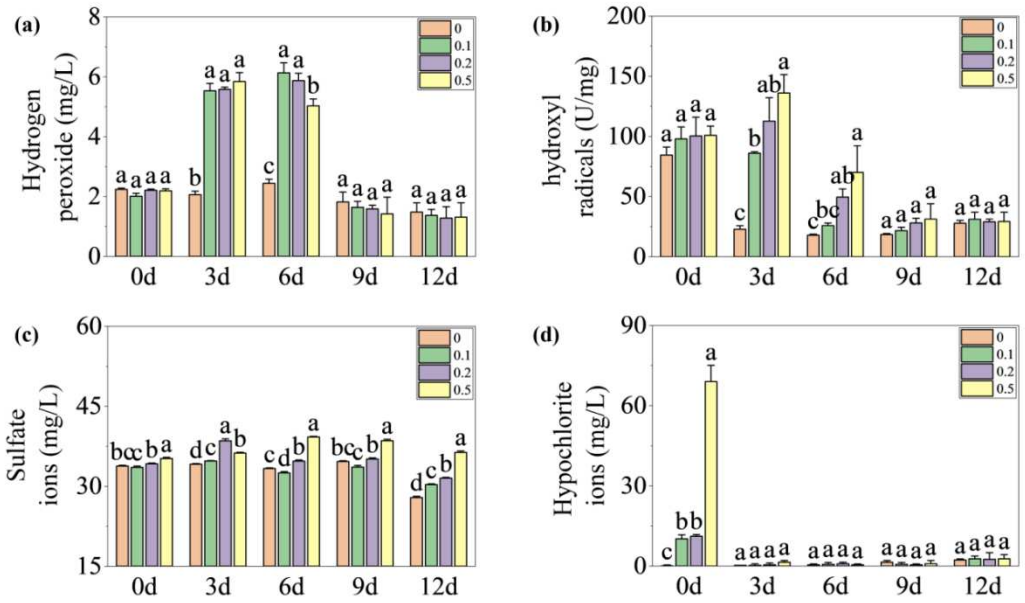


Fig. 5 Trends in the content of PMS decomposition products. All indicators shown in this figure were determined using their corresponding analytical methods, mainly colorimetric methods. (a) 0-12 d all group hydrogen peroxide (H_2O_2) content; (b) 0-12 d all group hydroxyl radical (•OH) content; (c) 0-12 d all group sulfate ion (SO_4^{2-}) content; (d) 0-12 d all group hypochlorite ion (ClO^-) content. A significance level of $P < 0.05$ was used for all comparisons.

3.7 Correlation normalization

To investigate the effects of PMS on various measured parameters in *C.pyrenoidosa*, a correlation heatmap analysis was conducted between PMS decomposition products (H_2O_2, •OH, SO_4^{2-}, and ClO^-) and the algal abundance, pigment content, intracellular particle content, and antioxidant enzyme activities of *C.pyrenoidosa.* The results showed while promoting chlorophyll fluorescence intensity, as well as MDA and ROS levels in *C.pyrenoidosa* (Fig. 6). Among these, the most significant correlations were observed between H_2O_2, and the inhibition of

chlorophyll b; •OH and the inhibition of chlorophyll a, algal abundance, and the activities of antioxidant enzymes (CAT, GSH-PX, SOD); SO_4^{2-} and the inhibition of chlorophyll a, algal abundance, and the activities of antioxidant enzymes (CAT, SOD); and ClO^- and the inhibition of intracellular particulate matter content and SOD activity (P<0.05). Furthermore, no significant correlations were identified between PMS decomposition products and the promotion of any related indicators.

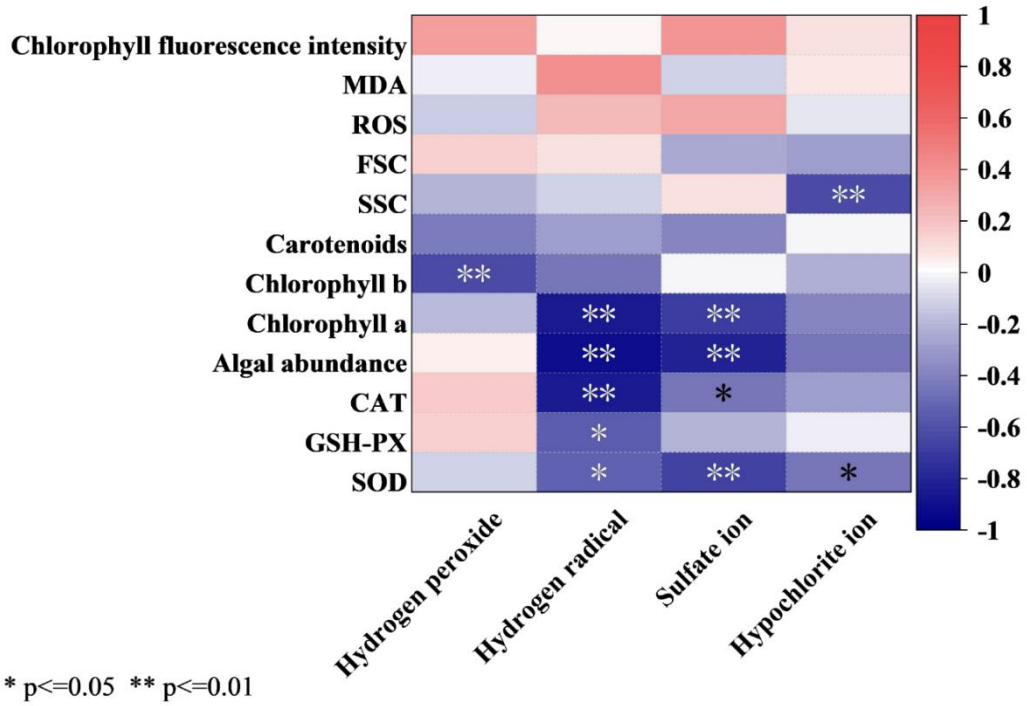


Fig. 6 Correlation heatmap between PMS decomposition products and physiological biochemical indexes of *C.pyrenoidosa.* After processing the data of PMS decomposition product concentrations and the various indicator data determined above, this figure was plotted using Origin.

3.8 high-throughput transcriptome sequencing

3.8.1 Screening and KEGG enrichment analysis of DEGs

To further investigate the response mechanism of *C.pyrenoidosa* cells to PMS stress, transcriptome analysis was performed on the experimental group and the control group to screen the differentially expressed genes (DEGs) in the experimental group compared with the control group. In the process of differential expression gene detection, |Fold Change |>2 and P-value <0.05 were used as the screening criteria. FC accounted for the ratio of expression amount among samples. In the process of differential expression analysis, the FDR correction method was also used to correct

the significant P-value obtained from the original hypothesis test, and finally value was used as the key index for differential expression gene screening (Dai et al., 2023).

Using the DEGs bar chart generated from control group of day 3 as a reference, the numbers of up-regulated genes in the experimental groups (ordered by increasing PMS concentration) were 171, 358, and 509, while the numbers of down-regulated genes were 581, 707, and 653, respectively (Fig. 7a). Principal component analysis (PCA) revealed that the gene expression pattern of the 0.5 × EC_{50} experimental group was markedly different from that of the control group, whereas the patterns of the 0.2 × EC_{50} and 0.1 × EC_{50} groups showed relatively minor differences from the control (Fig. 7b). As shown in the Venn diagram, the total numbers of DEGs in the experimental groups at day 3 were 752, 1,065, and 1,162 for increasing PMS concentrations, with 264 common DEGs shared among all experimental groups (Fig. 7c). The DEGs for each experimental group were also presented in the corresponding volcano plots (Fig. 7d-f). Taken together, these results indicate that at day 3 of cultivation, a clear dose-effect relationship exists between the number of DEGs and the PMS concentration; within a certain concentration range, higher PMS concentrations lead to a greater number of DEGs in *C.pyrenoidosa* cells.

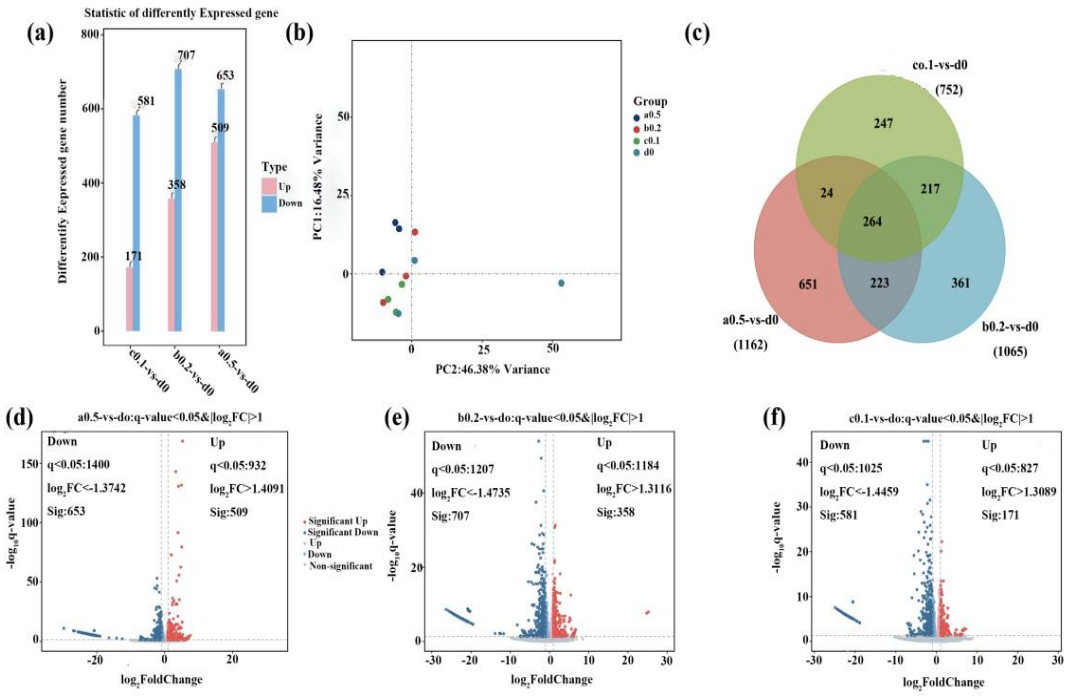


Fig. 7 Gene expression analysis of *C.pyrenoidosa* under the different concentrations of PMS on

day 3. All components of this figure were derived from the analysis of the day 3 high-throughput transcriptome sequencing data. (a) all experimental group differentially expressed genes (DEGs) number; (b) principal component analysis (PCA) figure; (c) Venn diagram of DEGs; (d-f) corresponding volcano plots. In the process of differential expression gene detection, |Fold Change |>2 and P-value <0.05 were used as the screening criteria.

The DEGs identified from comparing each concentration-based experimental group at day 3 with the control group at the same time point were mapped to KEGG pathways and functionally classified, with the results shown in Fig. 8. It could be seen that across all concentration groups, DEGs were generally significantly up-regulated in the functional category of translation (KO:03010), while being significantly down-regulated in carbohydrate metabolism (KO:00030) and in folding, sorting, and degradation (KO:04141).

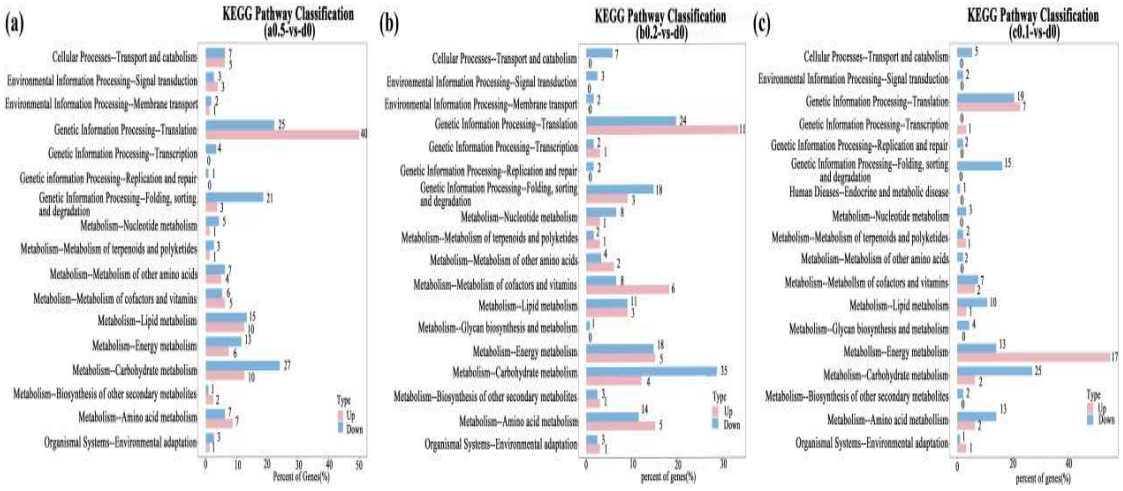


Fig. 8 The KEGG enrichment functional classification of DEGs between each experimental group and the control group at 3 days of cultivation. DEGs in each concentration-based experimental group after 3 days of cultivation were mapped to KEGG pathways.

To investigate the trend of DEGs changes in *C.pyrenoidosa* under continuous PMS stress, transcriptome analysis was performed on samples collected from the 0.5 × EC_{50} experimental group on days 0, 3, 6, 9, and 12 of cultivation, as well as on control group samples using day 0 as the reference. As shown in the DEG bar chart, the numbers of up-regulated genes in the experimental group were 415, 4,894, 8,345, 8,277, and 12,236, while the numbers of down-regulated genes were 1,404, 3,790, 4,168, 3,794, and 4,494, in chronological order of the sampling time points (Fig. 9a). Principal component analysis (PCA) revealed that the gene expression pattern of the

0.5 × EC_{50} experimental group was clearly distinct from that of the control group after day 0, and the difference became more lager at later sampling times (Fig. 9b). As shown in the Venn diagram, the total numbers of DEGs in the 0.5 × EC_{50} experimental group were 1,819, 8,684, 12,531, 12,071, and 16,730, corresponding to the sampling time points from early to late (Fig. 9c). The DEGs for each experimental group are also presented on the corresponding volcano plots (Fig. 9d-h). Collectively, these results indicate that following exposure to high-concentration PMS stress, *C.pyrenoidosa* cells initially produce a large number of down-regulated DEGs within a short period (0-3 days), followed by a rapid and sustained increase in up-regulated DEGs, whereas down-regulated DEGs show no distinct changes during the mid-to-late cultivation period (6-12 days).

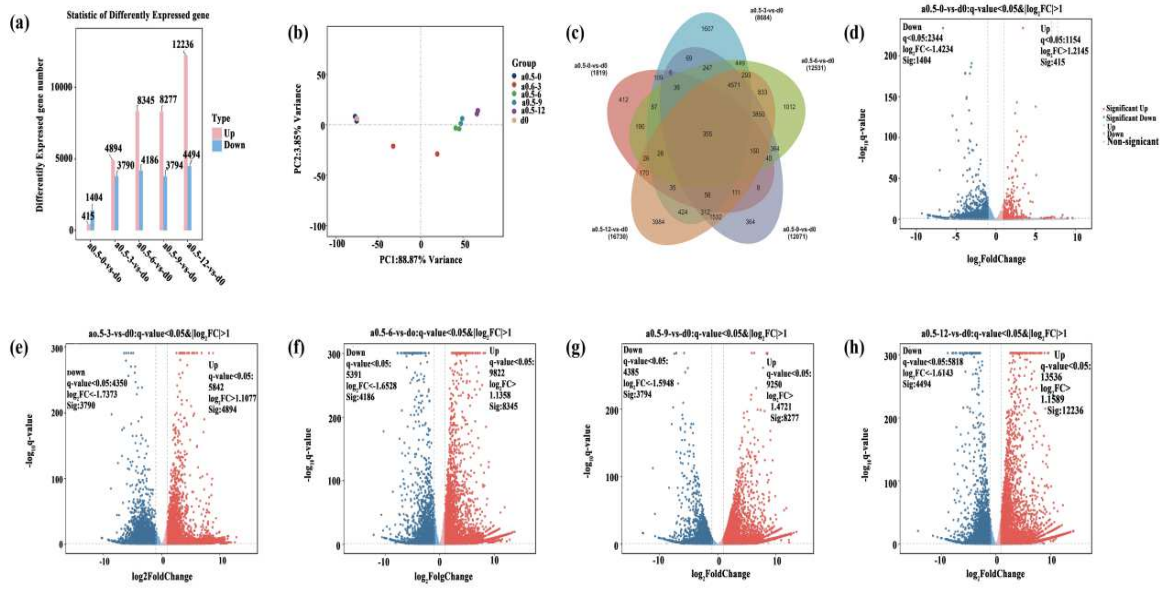


Fig. 9 Using the day 0 control group as a reference, gene expression of *C.pyrenoidosa* was analyzed from day 0 to day 12 under the 0.5 × EC_{50} experimental group condition. All components of this figure were derived from the analysis of the 0.5 × EC_{50} experimental group high-throughput transcriptome sequencing data. (a) the 0.5 × EC_{50} experimental group DEGs number; (b) PCA figure; (c) Venn diagram of DEGs; (d-h) corresponding volcano plots. In the process of differential expression gene detection, |Fold Change |>2 and P-value <0.05 were used as the screening criteria.

The DEGs obtained from comparing the 0.5 × EC_{50} experimental groups over 0-12 days with the control group at day 0 were mapped to KEGG pathways and

functionally classified, with the results presented in Fig. 10. In conjunction with Fig. 9a, it can be observed that the continuously increasing trend of up-regulated DEGs in the 0.5 × EC_{50} groups from day 3 to day 12 was primarily associated with functional categories related to translation (KO:03010), carbohydrate metabolism (KO:00030), amino acid metabolism (KO:00330), and transport and catabolism (KO:04145).

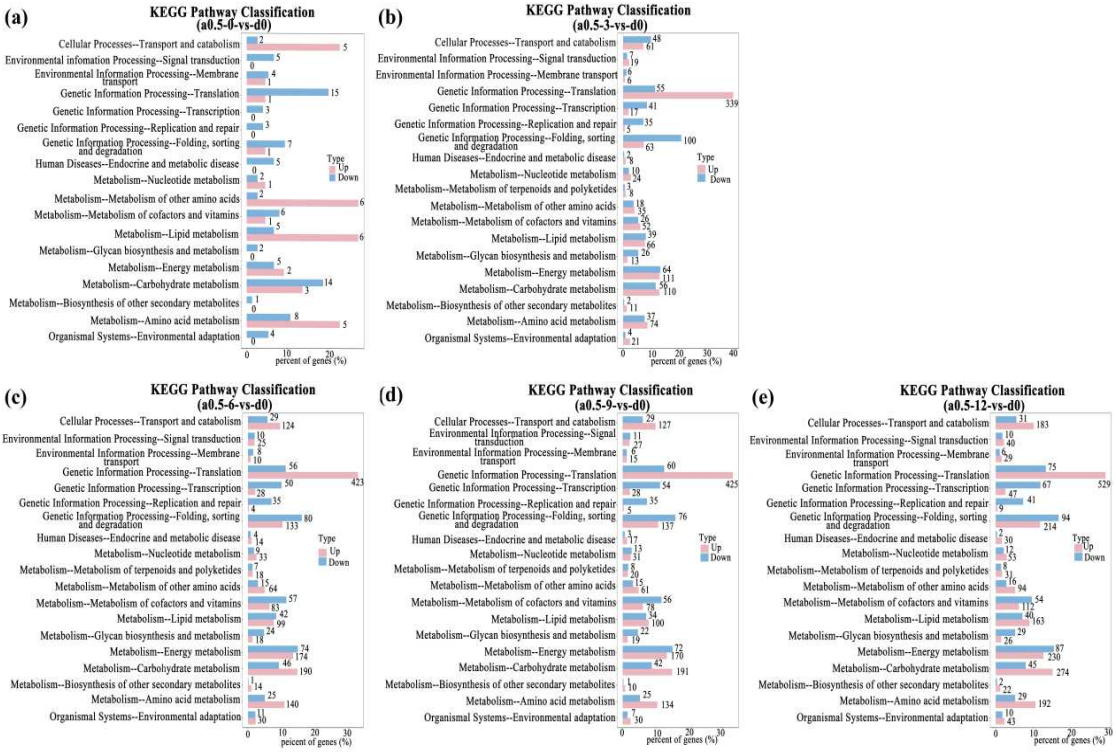


Fig. 10 The KEGG enrichment functional classification of DEGs between the 0.5 × EC_{50} experimental group at each sampling time point and the 0 d control group. DEGs in the 0.5 × EC_{50} experimental group after 0-12 days of cultivation were mapped to KEGG pathways.

3.8.2 GO Enrichment Analysis for Functional Classification of unigenes

The comparative go enrichment analysis showed that the most significant down-regulated genes in the biological process (BP), cell composition (CC) and molecular function (MF) of *C.pyrenoidosa* response to PMS stress in the experimental group were anchored component of plasma membrane (GO:0046658), water channel activity (GO:0015250), nutrient reservoir activity (GO:0045735), pyruvate metabolism (GO:0006090) and glucose metabolism (GO:0006006) (Fig. 11). By observing the above figure, it could be seen that the DEGs in the 0.2 × EC_{50} experimental group and 0.5 × EC_{50} experimental group is similar, and is significantly different from that in the low concentration group. Combined with the gene

expression analysis above, it could be considered that the low concentration PMS stress has little effect on the gene expression of *C.pyrenoidosa*.

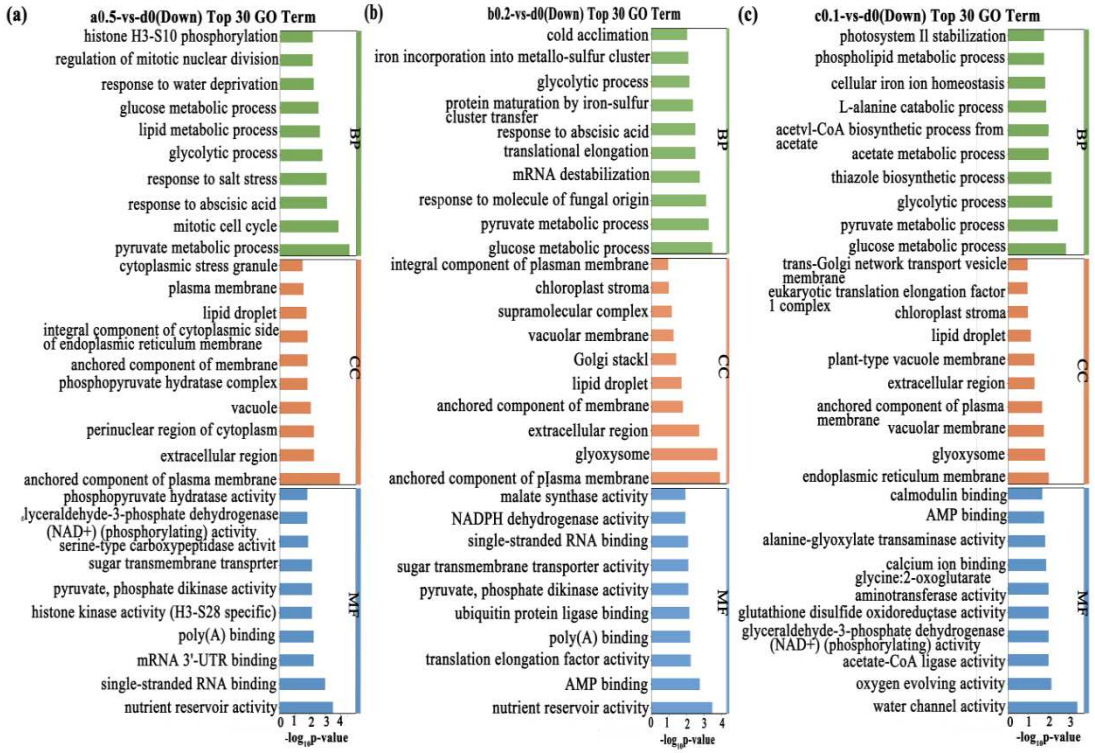


Fig. 11 The GO enrichment functional classification of DEGs between each experimental group and the control group at 3 days of cultivation. DEGs in each concentration-based experimental group after 3 days of cultivation were mapped to GO pathways.

It could be observed that for the 0.5 × EC_{50} experimental groups cultured from 3 to 12 days, the GO terms translation (GO:0006351), cytosolic large ribosomal subunit (GO:0022625), plasma membrane (GO:0005886), and structural constituent of ribosome (GO:0003735) were the most enriched functional categories among up-regulated DEGs in the three major GO classifications (cellular component, molecular function, and biological process), and were significantly more abundant than other functional groups (Fig. 12). Combined with the trend shown in Figure 10a, where the number of up-regulated DEGs in the 0.5 × EC_{50} group generally continued to increase from day 3 to day 12, it could be inferred that the additional up-regulated DEGs were primarily concentrated in these functional categories.

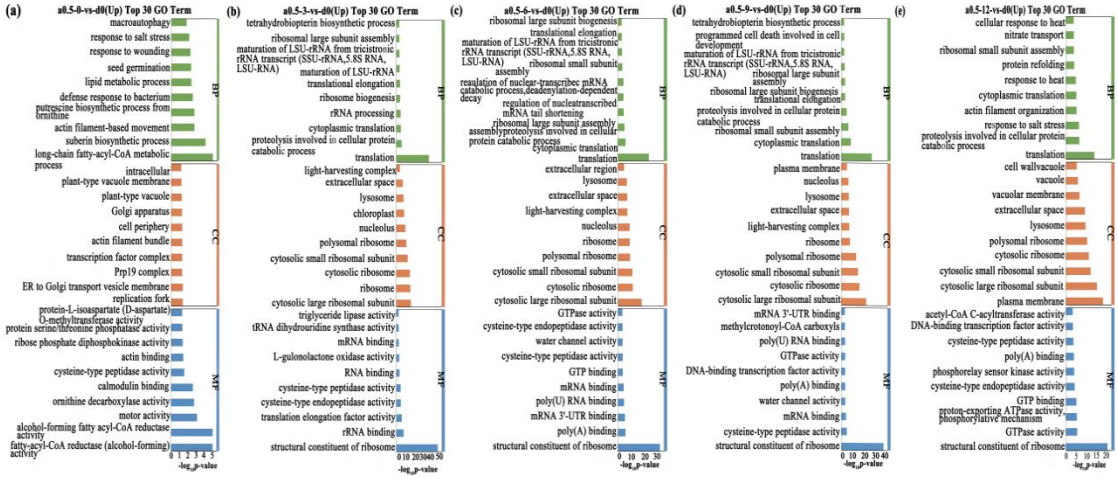


Fig. 12 The GO enrichment functional classification of DEGs between the 0.5 × EC_{50} experimental group at each sampling time point and the 0 d control group. DEGs in the 0.5 × EC_{50} experimental group after 0-12 days of cultivation were mapped to GO pathways.

4. Discussion

In this study, the toxic effects of PMS on *Chlorella pyrenoidosa* were investigated. The results demonstrated that the toxicity of PMS to *C.pyrenoidosa* is short-term, which is attributed to the rapid degradation of PMS and degradation products.

The acute toxicity of PMS to *C.pyrenoidosa* exhibits a positive correlation with PMS concentration. Upon activation, PMS generates a variety of reactive species that attack the algal cell membrane, elevate intracellular levels of reactive oxygen species (ROS), and excessively high ROS levels can damage cellular structures (Tian et al., 2024). Moreover, ROS can enter chloroplasts, leading to the degradation of photosynthetic pigments and disruption of the photosynthetic system, while also compromising the structure of antioxidant enzymes, thereby inhibiting their activities (Bai et al., 2004; Song et al., 2006). Out results showed that PMS damaged cell structure, photosynthetic pigments, antioxidant enzymes activity.

The decomposition products of PMS were further measured in this study, including H_2O_2, •OH, SO_4^{2-}, and ClO^-. H_2O_2 mainly attacks intracellular organelles, leading to mitochondrial deformation and increased endoplasmic reticulum (Darehshouri et al., 2008). It can also enter the chloroplasts of the cells that cause oxidative damage to the photosynthetic system, and induce lipid peroxidation that indirectly damage the antioxidant defense system (Ismaiel and Piercey-Normore, 2024; Moller et al., 2007). Hydroxyl radicals (•OH) not only impair cell surface structures via attacking hydrogen bonds and carbon chains of cellulose and pectin in

cell walls, damage chloroplasts by disrupting thylakoid membranes and inducing chlorophyll protein degradation (Wu et al., 2021), but also directly destroy the structure of antioxidant enzymes (Bai et al., 2004). Moreover, relevant studies have demonstrated that SO_4^{2-} inhibit the function of chloroplast photosystem II (PSII), thereby suppressing photosynthetic pigment content (Beauregard, 1991). It can also reduce the maximum electron transport rate, leading to the accumulation of excess electrons within cells (Chen et al., 2016). These surplus electrons react with oxygen, generating excessive ROS that surpass the cellular antioxidant capacity, thereby causing damage to the oxidative defense system. ClO^- primarily attacks the surface of algal cells, causing initial membrane damage and disruption of cellular structure, thereby creating conditions for subsequent more extensive oxidative stress (Cao et al., 2021). It interferes with the electron transport chain of photosystem II (PSII), leading to damage to photosystem II in *C.pyrenoidosa* cells, while also degrading photosynthetic pigments and reducing their content (N. Li et al., 2022). What's more, relevant studies have shown that ClO^- at certain concentrations can also directly disrupt the structure of antioxidant enzymes (Zhao et al., 2025). Through correlation analysis, our study also confirmed that these four decomposition products were correlated with photosynthetic pigments, antioxidant enzymes, and other parameters. Our results showed that the concentration of •OH generally significantly inhibited the photosynthetic pigments, growth performance, and antioxidant enzyme activities of *C.pyrenoidosa* cells, and the other detected decomposition products, especially SO_4^{2-}, exhibited similar trends. Moreover, previous studies have identified $SO_4^{\bullet-}$ and •OH as the primary reactive radicals contributing to the oxidative effects generated by PMS decomposition (Chen et al., 2021). Therefore, we speculate that $SO_4^{\bullet-}$ may also play a similar role throughout the entire period of stress exposure.

PMS rapidly decomposes into H_2O_2, •OH , SO_4^{2-}, and ClO^-. Among these, H_2O_2, •OH, and ClO^- also have their own decomposition cycles. When 1.6 mg L^{-1} H_2O_2 was added to the culture medium of *Aureococcus anophagefferens* (with cell densities ranging from 0.04 to 1.5 × 10^6 cells mL^{-1}), 70% to 98% of the H_2O_2 was decomposed into water and oxygen within 24 hours (Randhawa et al., 2014; Walling and Cleary, 1977). Relevant studies have shown that due to its high reactivity, the decomposition cycle of •OH in aqueous solution is on the order of microseconds, for example, with an average of 20.6 μs in rainwater (Arakaki et al., 1999). In addition, •OH can rapidly reacts with any accessible cellular components (Tafani et al., 2016). Therefore, once

the decomposition of PMS ceases to produce hydroxyl radicals, they rapidly react completely with nearby organic matter. Furthermore, due to its instability, ClO^- can decompose into chloride ions within 8 hours in a microalgal culture medium (Huang and Feng, 2025; Jeong et al., 2024). Among the decomposition products, SO_4^{2-} is relatively special in that it is not easily decomposed, and its concentration changes can be attributed to the complete decomposition of PMS and its absorption by *C.pyrenoidosa* cells (Hodson et al., 1971; Marahatta, 2021). In sum, it can be seen that the change in growth trend of *C.pyrenoidosa* in response to PMS decomposition stress in our results is reasonable.

PMS serves as a major disinfectant in aquaculture. Similarly, povidone-iodine, H_2O_2 and Benzalkonium chloride (BKC) are also widely applied for disinfection in this field. Relevant studies have shown that when *C.pyrenoidosa* is exposed to povidone-iodine within a certain concentration range (7-112 mg L^{-1}), the growth inhibition of the algal cells reaches its peak after 8 days of cultivation or later (Cao et al., 2022). Furthermore, when 60 μL of 15% H_2O_2 was added to a Petri dish (5.1 cm in diameter) culturing *Chlorella sp.*, the inhibition rate of chlorophyll a reached its peak after 10 days of cultivation, with a reduction of 86.3% in chlorophyll a content (Nikolic et al., 2021). Meanwhile, under the stress of 0.17 μl L^{-1} BKC, the cell density of *Chlorella sp.* only began to decrease rapidly after day 4 (Dũng et al., 2025). Compared with our results, it can be observed that the peak growth inhibition of *C.pyrenoidosa* cells under PMS stress is achieved relatively rapidly, which is also attributed to the oxidative stress induced by the substances generated from the rapid decomposition of PMS.

Transcriptomic gene analysis on day 3 demonstrated that the number of differentially expressed genes (DEGs) in experimental groups was positively correlated with PMS concentration. This is generally consistent with the transcriptomic gene expression trends reported in relevant studies, indicating that this is a defense response strategy of *C.pyrenoidosa* under PMS stress (Chávez Montes et al., 2024). *C.pyrenoidosa* in all concentration groups exhibited up-regulation of DEGs primarily in functional categories related to translation, while down-regulation was observed in categories associated with the anchored component of plasma membrane, nutrient reservoir activity, pyruvate metabolism, glucose metabolism, carbohydrate metabolism, and folding, sorting, and degradation. Down-regulation of

nutrient-reservoir-associated pathways (e.g., pyruvate, glucose, and carbohydrate metabolism) impairs cellular energy metabolism, thereby inducing morphological and growth alterations such as abnormal cell volume and membrane damage, which aligns with and corroborates the findings described above (Li et al., 2025). The down-regulation of plasma membrane anchoring component pathways prevents membrane proteins from anchoring to their appropriate sites, thereby compromising the stability, integrity, and signaling functions of the cell membrane (Chun et al., 2022). Integrated with the experimental group data, it could be concluded that the surface wrinkling and deformation observed in *C.pyrenoidosa* cells are caused by the down-regulation of plasma membrane anchoring pathways, and that the impairment of membrane function further inhibited the growth of *C.pyrenoidosa* cells (Simons and Sampaio, 2011). The primary function of the folding, sorting, and degradation pathways is to assist in the correct folding of nascent polypeptide chains, prevent their aggregation, identify and sort misfolded proteins, and facilitate either their refolding or targeted degradation (Kim et al., 2013). Therefore, the down-regulation of folding, sorting, and degradation pathways led to the accumulation of misfolded polypeptides in *C.pyrenoidosa* cells, impairing and decelerating protein synthesis. This subsequently induced endoplasmic reticulum stress and dysfunction, which was consistent with our previous observations from transmission electron microscopy. Furthermore, according to relevant studies, the up-regulation of translation-related genes is aimed at synthesizing repair- and defense-related proteins to repair and mitigate the oxidative damage incurred (Chen et al., 2024). This was also validated by subsequent transcriptome analysis results and the growth trends of *C.pyrenoidosa* cells.

Furthermore, our transcriptomic results showed that under varying PMS stress duration, DEGs in all experimental group were down-regulated on day 3 in categories related to anchored component of plasma membrane and carbohydrate metabolism, but generally up-regulated on days 6-12 in the 0.5 × EC_{50} group in these same categories, indicating algal adaptation and self-recovery under PMS stress. In the 0.5 ×EC_{50} group, up-regulated DEGs during days 6-12 were enriched in ribosomal pathways (translation, carbohydrate metabolism, plasma membrane, cytosolic large ribosomal subunit, structural constituent of ribosome, amino acid metabolism,and

606 transport and catabolism). Study has shown indicating that ribosome up-regulation
607 enhanced translational quality control, accelerated protein synthesis, and promoted
608 cellular repair, which is consistent with the results of our phenotypic experiments
609 (Inada, 2017). Therefore, our transcriptomic data were highly consistent with
610 physiological and biochemical indicators and growth curves, supporting that
611 expression trends from two replicates reflect genuine biological processes. Given that
612 increasing replicates enhances detection power more than sequencing depth in
613 high-dose RNA-seq, and key GO pathways are reliably detectable with two replicates
614 (Rasim Barutcu, 2024), prioritizing replicates at critical time points (e.g., day 3) while
615 using fewer at others yields robust biological insights. Based on DEG functional
616 classification, the mechanism underlying the initial growth inhibition followed by
617 recovery in *C.pyrenoidosa* under PMS stress is as follows: early oxidative stress
618 down-regulates nutrient/growth-related genes and up-regulates translation-related
619 genes for repair; later, as stress subsides, anabolism is reactivated to restore growth.
620 This pattern exemplifies the classic "growth-defense trade-off" at the transcriptional
621 level (Huot et al., 2014).

622 As a multifunctional microalga widely used in aquaculture, *C.pyrenoidosa* is
623 subject to toxic effects during PMS disinfection, which will undoubtedly reduce the
624 productivity of aquaculture water bodies. Combined with previous findings indicate
625 that within the tested concentration range, the inhibition of primary productivity in
626 aquaculture water bodies by PMS is short-term and reversible; sufficient recovery
627 intervals should be ensured to avoid cumulative stress on algal functional
628 communities. Although the 96 h EC_{50} of PMS for *C.pyrenoidosa* was 16.98 mg L^{-1},
629 slight growth inhibition and oxidative stress were still observed even in the 1.70
630 mg L^{-1} experimental group of this study, particularly on day 3 of cultivation. In this
631 way, it is recommended that the single application concentration of PMS in
632 aquaculture be controlled below 1.7 mg L^{-1} (0.1 × EC_{50}), and that application of
633 *C.pyrenoidosa* should avoid the peak toxicity period caused by the decomposition of
634 PMS products (day 3). In addition, six days after PMS application, as the
635 decomposition products are exhausted, the toxic effects on microalgae will naturally

diminish, and algal cell productivity can recover without additional intervention; thereafter, the production function of *C.pyrenoidosa* will not be affected when it is applied.

5.Conclusion

This study systematically investigated the toxic effects of potassium monopersulfate (PMS) on the multifunctional microalga *C.pyrenoidosa* in aquaculture water bodies and the underlying mechanisms, and on this basis assessed the trend of PMS effects on the primary productivity of water bodies in aquaculture practice. Exposure to PMS markedly suppressed the growth of *C.pyrenoidosa*, decreased the contents of photosynthetic pigments, disrupted chlorophyll fluorescence, and induced damage to cellular ultrastructure. Such toxic responses were accompanied by increased levels of reactive oxygen species (ROS) and malondialdehyde (MDA), along with reduced activities of catalase (CAT), superoxide dismutase (SOD) and glutathione peroxidase (GSH-PX). The observed toxicity was primarily derived from PMS degradation products, showing an acute short-term response that peaked on day 3, followed by a gradual recovery. This recovery trend can be explained by the rapid degradation of PMS and the instability of its byproducts. Transcriptomic analysis further elucidated the response mechanism of *C.pyrenoidosa* under PMS stress. Upon oxidative stress, the algal down-regulated cell growth and metabolic processes to prioritize the synthesis of defense-related proteins, thus the algal slowed cell growth and metabolism to prioritize defense-related protein synthesis, thereby mitigating oxidative damage. Once oxidative stress was alleviated, metabolic activity was enhanced to restore cellular growth. As noted above, the time-dependent toxicity of PMS to *C.pyrenoidosa* observed in this study, driven by the dynamic changes in PMS decomposition product concentrations, is of considerable importance for accurately evaluating the impact of PMS on the primary productivity of aquaculture water bodies and its ecological risk window in aquaculture practice.

Declarations

CRediT authorship contribution statement

Yi Du: Writing – review & editing, Writing – original draft, Visualization, Investigation, Data curation, Conceptualization. Le kong: Visualization, Investigation, Data curation. Qiyan Cao: Validation, Investigation, Formal analysis. Haiyong Zhao: Methodology, Conceptualization. Wenzhi Wei: Writing – review & editing, Writing – original draft, Methodology, Investigation, Funding acquisition.

Funding

The authors did not receive support from any organization for the submitted work.

Competing interest

Our have no known competing financial interests or personal relationships that could have appeared to influence the work reported in this paper.

Data availability

The data that support the findings of this study are available from the corresponding author upon reasonable request.

Reference:

Adachi, A., Faiçal El, O., Mohammed, K., Ibtissam El, M., Assouguem, A., Almutairi, M. H.,…Lahkimi, A. (2022). Decolorization and Degradation of Methyl Orange Azo Dye i n Aqueous Solution by the Electro Fenton Process: Application of Optimization. Cataly sts, 12(6), 665. https://doi.org/https://doi.org/10.3390/catal12060665

Anipsitakis, G. P., Tufano, T. P., & Dionysiou, D. D. (2008). Chemical and microbial deconta mination of pool water using activated potassium peroxymonosulfate. Water Research, 42(12), 2899-2910. https://doi.org/https://doi.org/10.1016/j.watres.2008.03.002

Arakaki, T., Miyake, T., Shibata, M., & Sakugawa, H. (1999). Photochemical formation and sc avenging of hydroxyl radical in rain and dew waters. Nippon Kagaku Kaishi(5), 335-3 40. https://doi.org/10.1246/nikkashi.1999.335

Bai, X., Xue, X., Bai, M., Yang, B., & Zhang, Z. (2004). Biochemistry Effects Of Hydroxyl Radicals to Invasive Marine Species. In S. Keping & Y. Gefei (Eds.), Recent Developments in Applied Electrostatics (pp. 212-215). Elsevier Science Ltd. https://doi.org/https://doi.org/10.1016/B978-008044584-7.50055-4

Beauregard, M. (1991). Involvement of sulfite and sulfate anions in the SO_2^- induced inhibition of the oxygen evolving enzyme photosystem II in chloroplasts: A review. Environmental And Experimental Botany, 31(1), 11-21. https://doi.org/https://doi.org/10.1016/0098-8472(91)90003-7

Cao, Q., Jiang, Y., Yang, H., Zhang, Y., & Wei, W. (2022). Comprehensive toxic effects of povidone iodine on microalgae Chlorella pyrenoidosa under different concentrations. Aquaculture Research, 53(5), 1833-1841. https://doi.org/https://doi.org/10.1111/are.15711

Cao, S., Zhang, D., Teng, F., Liao, R., Cai, Z. H., Tao, Y., & Hu, H. Y. (2021). Inhibitory effects of ultralow-dose sodium hypochlorite on Microcystis aeruginosa and Chlorella vulgaris: Differences in sensitivity and physiology. Science of The Total Environment, 774, Article 145638. https://doi.org/10.1016/j.scitotenv.2021.145638

Cao, Y., Yang, S., Wang, J., Kong, W., Guo, B., Xi, Y.,…Yue, B. (2023). Metabolomic exploration of the physiological regulatory mechanism of the growth and metabolism characteristics of Chlorella vulgaris under photoautotrophic, mixotrophic, and heterotrophic cultivation conditions. Biomass And Bioenergy, 173, 106775. https://doi.org/https://doi.org/10.1016/j.biombioe.2023.106775

Chávez Montes, R. A., Mary, M. A., Rashel, R. H., Fokar, M., Herrera-Estrella, L., Lopez-Arredondo, D., & Patiño, R. (2024). Hormetic and transcriptomic responses of the toxic alga Prymnesium parvum to glyphosate. Science of The Total Environment, 954, 176451. https://doi.org/https://doi.org/10.1016/j.scitotenv.2024.176451

Chen, L., Gin, K. Y. H., & He, Y. L. (2016). Effects of sulfate on microcystin production, photosynthesis, and oxidative stress in Microcystis aeruginosa. Environmental Science And Pollution Research, 23(4), 3586-3595. https://doi.org/10.1007/s11356-015-5605-1

Chen, Z., Li, J., Chen, M., Koh, K. Y., Du, Z., Gin, K. Y.-H.,…Chen, J. P. (2021). Microcystis aeruginosa removal by peroxides of hydrogen peroxide, peroxymonosulfate and peroxydisulfate without additional activators. Water Research, 201, 117263. https://doi.org/https://doi.org/10.1016/j.watres.2021.117263

Chen, Z. F., Shi, C. H., & Liu, A. (2024). Toxicity of urban stormwater on Chlorella pyrenoidosa: Implications for reuse safety. Science of The Total Environment, 926, Article 171803. https://doi.org/10.1016/j.scitotenv.2024.171803

Chun, J., Ko, Y.-H., So, K.-K., Cho, S.-H., & Kim, D.-H. (2022). A fungal GPI-anchored protein gene functions as a virulence and antiviral factor. Cell Reports, 41(2), 111481. https://doi.org/https://doi.org/10.1016/j.celrep.2022.111481

Dai, J. X., Zheng, M. M., He, Y. J., Zhou, Y. C., Wang, M. Z., & Chen, B. L. (2023). Real-time response counterattack strategy of tolerant microalgae Chlorella vulgaris MBFJNU-1 in original swine wastewater and free ammonia. Bioresource Technology, 377, Article 128945. https://doi.org/10.1016/j.biortech.2023.128945

Damergi, E., Schwitzguébel, J.-P., Refardt, D., Sharma, S., Holliger, C., & Ludwig, C. (2017). Extraction of carotenoids from Chlorella vulgaris using green solvents and syngas prod

uction from residual biomass. Algal Research, 25, 488-495. https://doi.org/https://doi.org/10.1016/j.algal.2017.05.003

Darehshouri, A., Affenzeller, M., & Lütz-Meindl, U. (2008). Cell death upon H_2O_2 induction in the unicellular green alga Micrasterias. Plant Biology, 10(6), 732-745. https://doi.org/https://doi.org/10.1111/j.1438-8677.2008.00078.x

Deng, Y., Chen, F. F., Liao, K., Xiao, Y., Chen, S. H., Lu, Q.,…Zhou, W. G. (2021). Microalgae for nutrient recycling from food waste to aquaculture as feed substitute: a promising pathway to eco-friendly development.Journal of Chemical Technology And Biotechnology, 96(9), 2496-2508. https://doi.org/10.1002/jctb.6786

Dũng, L., Vững, Đ. V., Vân, L., & Hồng, P. (2025). ẢNH HƯỞNG CỦA VI SINH VÀ BENZALKONIUM CHLORINE LÊN SINH TRƯỞNG CỦA VI TẢO LỤC VÀ VI KHUẨN LAM NƯỚC NGỌT. Tạp chí Khoa học Nông nghiệp Việt Nam, 23(10), 1292-1300. https://doi.org/10.31817/tckhnnvn.2025.23.10.02

FDMA. 2025. China Fisheries Statistical Yearbook (2024). China Agriculture Press.

Ganguly, J., Tempelaars, M., Abee, T., & van Kranenburg, R. (2020). Characterization of sporulation dynamics of Pseudoclostridium thermosuccinogenes using flow cytometry. Anaerobe, 63, 102208. https://doi.org/https://doi.org/10.1016/j.anaerobe.2020.102208

Hao, Y., Lu, S., Chu, G., & Gao, M. (2025). Effect of salinity on nitrogen removal performance, enzymatic activity and metabolic pathway of Chlorella pyrenoidosa treating aquaculture wastewater. Environmental Research, 265, 120405. https://doi.org/https://doi.org/10.1016/j.envres.2024.120405

Hodson, R. C., Schiff, J. A., & Mather, J. P. (1971). Studies of Sulfate Utilization by Algae: 10. Nutritional and Enzymatic Characterization of Chlorella Mutants Impaired for Sulfate Utilization 1. Plant Physiology, 47(2), 306-311. https://doi.org/10.1104/pp.47.2.306

Huang, Y., & Feng, K. (2025). Application of the MW/Co_2^+/PMS process in the treatment of high-chloride mature leachate: A study of the removal characteristics of ammonia nitrogen and organic matter. Journal of Environmental Chemical Engineering, 13(2), 115955. https://doi.org/https://doi.org/10.1016/j.jece.2025.115955

Huot, B., Yao, J., Montgomery, B. L., & He, S. Y. (2014). Growth-Defense Tradeoffs in Plants: A Balancing Act to Optimize Fitness. Molecular Plant, 7(8), 1267-1287. https://doi.org/10.1093/mp/ssu049

Inada, T. (2017). The Ribosome as a Platform for mRNA and Nascent Polypeptide Quality Control. Trends In Biochemical Sciences, 42(1), 5-15. https://doi.org/10.1016/j.tibs.2016.09.005

Ismaiel, M. M. S., & Piercey-Normore, M. D. (2024). Cooperative antioxidative defense of the blue-green alga Arthrospira (Spirulina) platensis under oxidative stress imposed by exogenous application of hydrogen peroxide. Environmental Pollution, 341, 123002. https://doi.org/https://doi.org/10.1016/j.envpol.2023.123002

Jeong, S. H., Kim, W., & Kwon, J. H. (2024). Development of a new sterilization method for microalgae media using calcium hypochlorite as the sterilant. Bioprocess And Biosystems Engineering, 47(3), 393-401. https://doi.org/10.1007/s00449-024-02971-z

Johnston, A. E., Shavalier, M. A., Scribner, K. T., Soto, E., Yun, S. S., & Loch, T. P. (2024). Assessing the Efficacy of Three Hatchery Disinfectants for the Inactivation of a Lake

Sturgeon Herpesvirus (Family: Alloherpesviridae). Viruses-Basel, 16(7), Article 1062. https://doi.org/10.3390/v16071062

Kim, Y. E., Hipp, M. S., Bracher, A., Hayer-Hartl, M., & Hartl, F. U. (2013). Molecular Chaperone Functions in Protein Folding and Proteostasis. In R. D. Kornberg (Ed.), Annual Review of Biochemistry, VOL 82 (Vol. 82, pp. 323-355). https://doi.org/10.1146/annurev-biochem-060208-092442

Li, N., Liu, Z., Wang, P., Suman, K., Zhang, J., & Song, Y. (2022). Effects of sodium hypochlorite treatment on the chlorophyll fluorescence in photosystem II of microalgae. Science of The Total Environment, 833, 155192. https://doi.org/https://doi.org/10.1016/j.scitotenv.2022.155192

Li, Z., Dong, S., Huang, F., Lin, L. L., Hu, Z. L., & Zheng, Y. H. (2022). Toxicological Effects of Microplastics and Sulfadiazine on the Microalgae Chlamydomonas reinhardtii. Frontiers In Microbiology, 13, Article 865768. https://doi.org/10.3389/fmicb.2022.865768

Li, Z., Wang, X. L., Ren, M. Y., Li, Z. Y., Xi, Y. Q., Su, L. J.,…Yin, X. M. (2025). Sublethal and lethal effects of avermectin on reproductive success, hormonal regulation, and population dynamics of the oriental fruit fly, Bactrocera dorsalis. Pest Management Science, 81(9), 5458-5469. https://doi.org/10.1002/ps.8899

Liu, L., Zhang, S. L., Dai, W., Bi, X. D., & Zhang, D. J. (2019). Comparing effects of berberine on the growth and photosynthetic activities of Microcystis aeruginosa and Chlorella pyrenoidosa. Water Science And Technology, 80(6), 1155-1162. https://doi.org/10.2166/wst.2019.357

Liu, Y., Xu, W., Zhao, L., Wang, Y., & Zhang, J. (2017). Absorption of NO and Simultaneous Absorption of SO_2/NO Using a Vacuum Ultraviolet Light/Ultrasound/$KHSO_5$ System. Energy & Fuels, 31(11), 12364-12375. https://doi.org/10.1021/acs.energyfuels.7b01274

Luo, H., Liu, C., Cheng, Y., Zeng, Y., He, D., & Pan, X. (2021). Fe(III) greatly promotes peroxymonosulfate activation by WS2 for efficient carbamazepine degradation and Escherichia coli disinfection. Science of The Total Environment, 787, 147724. https://doi.org/https://doi.org/10.1016/j.scitotenv.2021.147724

Marahatta, A. B. (2021). Chemical Energetics and Atomic Charges Distribution of Variably Sized Hydrated Sulfate Clusters in the light of Density Functional Theory. International Journal of Progressive Sciences And Technologies, 25(1), 10. https://doi.org/10.52155/ijpsat.v25.1.2690

Maxwell, K., & Johnson, G. N. (2000). Chlorophyll fluorescence—a practical guide. Journal of Experimental Botany, 51(345), 659-668. https://doi.org/10.1093/jexbot/51.345.659

Mohammadi, S., Moussavi, G., Shekoohiyan, S., Marín, M. L., Boscá, F., & Giannakis, S. (2021). A continuous-flow catalytic process with natural hematite-alginate beads for effective water decontamination and disinfection: Peroxymonosulfate activation leading to dominant sulfate radical and minor non-radical pathways. Chemical Engineering Journal, 411, 127738. https://doi.org/https://doi.org/10.1016/j.cej.2020.127738

Moller, I. M., Jensen, P. E., & Hansson, A. (2007). Oxidative modifications to cellular components in plants. Annual Review of Plant Biology, 58, 459-481. https://doi.org/10.1146/annurev.arplant.58.032806.103946

826 Ng, M. K., & Mont, M. A. (2025). Beyond quaternary ammonium compounds: Evaluating the
827 harms of non-QAC disinfectant agents in healthcare and industry. GMS Hygiene And I
828 nfection Control, 20, Article dgkh000591. https://doi.org/10.3205/dgkh000591
829 Nikolic, N., Simic, G. S., Golic, I., & Popovic, S. (2021). The effects of biocides on the gro
830 wth of aerophytic green algae (Chlorella sp.) isolated from a cave environment. Archiv
831 es of Biological Sciences, 73(3), 341-351. https://doi.org/10.2298/ABS210321027N
832 Peng, P., Li, J., Zhou, H., Yang, X., Wu, M., Zhang, Y., & Zhan, J. (2025). Allelopathy and
833 underlying mechanism of Chlorella pyrenoidosa on the bloom-causing dinoflagellate He
834 terocapsa bohaiensis. Algal Research, 85, 103828. https://doi.org/https://doi.org/10.1016/j.
835 algal.2024.103828
836 Randhawa, V., Thakkar, M., & Wei, L. P. (2014). Effect of Aureococcus anophagefferens biom
837 ass on its inactivation by hydrogen peroxide: culture study and empirical modeling. Jo
838 urnal of Applied Phycology, 26(1), 349-355. https://doi.org/10.1007/s10811-013-0107-3
839 Rasim Barutcu, A. (2024). Evaluation of Replicate Number and Sequencing Depth in Toxicolog
840 y Dose-Response RNA-seq. Computational Toxicology, 30, 100307. https://doi.org/https:/
841 /doi.org/10.1016/j.comtox.2024.100307
842 Salami, F. H., Bonifacio, V., de Oliveira, G. G., & Fatibello, O. (2008). Spectrophotometric M
843 ulticommutated Flow System for the Determination of Hypochlorite in Bleaching Produ
844 cts. Analytical Letters, 41(17), 3187-3197, Article Pii 906645917. https://doi.org/10.1080
845 /00032710802462925
846 Santiago-Espiñeira, P., García-Muñoz, P., Campayo-Navarro, P., & Rodríguez-Chueca, J. (2025).
847 Harnessing UV-C photoassisted AOPs: Amoxicillin degradation, disinfection by-product
848 s formation, and Enterococcus faecalis inactivation in aquaculture water. Journal of En
849 vironmental Management, 388, 125983. https://doi.org/https://doi.org/10.1016/j.jenvman.20
850 25.125983
851 Simons, K., & Sampaio, J. L. (2011). Membrane Organization and Lipid Rafts. Cold Spring H
852 arbor Perspectives In Biology, 3(10), Article a004697. https://doi.org/10.1101/cshperspect.
853 a004697
854 Song, Y. G., Liu, B., Wang, L. F., Li, M. H., & Liu, Y. (2006). Damage to the oxygen-evolvi
855 ng complex by superoxide anion, hydrogen peroxide, and hydroxyl radical in photoinhi
856 bition of photosystem II. Photosynthesis Research, 90(1), 67-78. https://doi.org/10.1007/s
857 11120-006-9111-7
858 Tafani, M., Sansone, L., Limana, F., Arcangeli, T., De Santis, E., Polese, M.,…Russo, M. A.
859 (2016). The Interplay of Reactive Oxygen Species, Hypoxia, Inflammation, and Sirtuins
860 in Cancer Initiation and Progression. Oxidative Medicine And Cellular Longevity, 201
861 6, Article 3907147. https://doi.org/10.1155/2016/3907147
862 Tian, N., Schmidt, L. C., Lameiro, M. J. A., Polo-López, M. I., Marín, M. L., Boscá, F.,…Gia
863 nnakis, S. (2024). Why is $HSO5^-$ so effective against bacteria? Insights into the mecha
864 nisms of Escherichia coli disinfection by unactivated peroxymonosulfate. Water Researc
865 h, 254, 121441. https://doi.org/https://doi.org/10.1016/j.watres.2024.121441
866 Vijayakumar, P., & Dawson, P. A. (2024). Analytical methods for quantitating sulfate in plasma
867 and serum. Essays Biochem, 68(4), 383-389. https://doi.org/10.1042/ebc20230092
868 Vishwakarma, R., Dhar, D. W., Jena, M., & Shukla, M. (2023). Pigment composition analysis
869 of selected green microalgae through multivariate analysis and their potential as high v

alue nutraceuticals. Vegetos, 36(4), 1496-1508. https://doi.org/10.1007/s42535-022-00562-5

Walling, C., & Cleary, M. (1977). Oxygen evolution as a critical test of mechanism in the ferric-ion catalyzed decomposition of hydrogen peroxide. International Journal of Chemical Kinetics, 9, 595-601. https://doi.org/10.1002/kin.550090408

Wang, J. Y., Yu, Y. G., & Dong, Y. M. (2020). Combination of polyhexamethylene guanidine hydrochloride and potassium peroxymonosulfate to disinfect ready-to-eat lettuce. RSC Advances, 10(66), 40316-40320. https://doi.org/10.1039/d0ra08356a

Wu, Y., Xiang, W., Li, L., Liu, H., Zhong, N., Chang, H., & Rittmann, B. E. (2021). A novel photoelectrochemical system to disrupt microalgae for maximizing lipid-extraction efficiency. Chemical Engineering Journal, 420, 130517. https://doi.org/https://doi.org/10.1016/j.cej.2021.130517

Xiang, Q., & Zhou, Y. (2023). Enantioselective Toxic Effects of Prothioconazole toward Scenedesmus obliquus. Molecules, 28(12), 4774. https://doi.org/10.3390/molecules28124774

Xu, C., Su, G., Zhao, K., Kong, X., Wang, H., Xu, X.,…Xu, J. (2023). Societal benefits and environmental performance of Chinese aquaculture. Journal of Cleaner Production, 422, 138645. https://doi.org/https://doi.org/10.1016/j.jclepro.2023.138645

Yin, P., Wang, D., Zhang, X., Zhang, G., Zhao, H., Zhang, Y., & Yang, H. (2026). Effects of KMPS on eutrophic sediment-water interface in pond aquaculture: Based on physicochemical properties, DOM characteristics and microbial community structure. Aquaculture, 612, 743089. https://doi.org/https://doi.org/10.1016/j.aquaculture.2025.743089

Yu, W., Pan, T., Yu, Y., Wu, Y., Pan, Y., & Yang, X. (2020). A novel peroxymonosulfate (PMS)-enhanced iron coagulation process for simultaneous removal of trace organic pollutants in water. Water Research, 185, 116136. https://doi.org/https://doi.org/10.1016/j.watres.2020.116136

Zeng, J., Tian, J., Kan, D., Han, C., Fei, X., Ma, X.,…Ge, J. (2023). Study of filtration, digestion and absorption of Chlorella pyrenoidosa by juvenile Chinese mitten crab (Eriocheir sinensis). Aquaculture, 575, 739772. https://doi.org/https://doi.org/10.1016/j.aquaculture.2023.739772

Zhang, L., Zhang, Y., Qian, Y., Qin, C., Li, H., & Tang, J. (2025). Revealing the main toxic factor and mechanisms of shale gas flowback water on the growth of algae Chlorella pyrenoidosa. Environment International, 202, 109654. https://doi.org/https://doi.org/10.1016/j.envint.2025.109654

Zhao, J., Cao, X., Wang, Z., Dai, Y., & Xing, B. (2017). Mechanistic understanding toward the toxicity of graphene-family materials to freshwater algae. Water Research, 111, 18-27. https://doi.org/https://doi.org/10.1016/j.watres.2016.12.037

Zhao, L. J., Tan, C. X., Tang, Y. T., Zhang, Z., Guo, L. X., Yao, G. Y.,…Qian, C. (2025). The Synergistic Effect of Sodium Hypochlorite (NaClO) and Organosilicone Adjuvant Enhances the Inhibition and Oxidative Damage in Cladophora sp. Biology-Basel, 14(12), Article 1773. https://doi.org/10.3390/biology14121773

Zhao, W., & Shen, H. (2016). A statistical analysis of China's fisheries in the 12th five-year period. Aquaculture And Fisheries, 1, 41-49. https://doi.org/https://doi.org/10.1016/j.aaf.2016.11.001

Zheng, X., Niu, X., Zhang, D., Lv, M., Ye, X., Ma, J.,…Fu, M. (2022). Metal-based catalysts for persulfate and peroxymonosulfate activation in heterogeneous ways: A review. Chemical Engineering Journal, 429, 132323. https://doi.org/https://doi.org/10.1016/j.cej.2021.132323

Zhou, G. J., Peng, F. Q., Zhang, L. J., & Ying, G. G. (2012). Biosorption of zinc and copper from aqueous solutions by two freshwater green microalgae Chlorella pyrenoidosa and Scenedesmus obliquus. Environmental Science And Pollution Research, 19(7), 2918-2929. https://doi.org/10.1007/s11356-012-0800-9

Zou, J., Cai, H. H., Wang, D. Y., Xiao, J. Y., Zhou, Z. M., & Yuan, B. L. (2019). Spectrophotometric determination of trace hydrogen peroxide via the oxidative coloration of DPD using a Fenton system. Chemosphere, 224, 646-652. https://doi.org/10.1016/j.chemosphere.2019.03.005

Supplementary Files

This is a list of supplementary files associated with this preprint. Click to download.

- Highlights.docx
- Rawdataofthestudiedphenotypicindicators.xlsx